Magnetic FEM Design and Experimental Validation of an Innovative Fail-Safe Magnetorheological Clutch Excited by Permanent Magnets

Rocco Rizzo, Antonino Musolino, Francesco Bucchi, Paola Forte, and Francesco Frendo

***Abstract*—This paper describes the magnetic design of an innovative fail-safe clutch based on magnetorheological fluid (MRF). A cylindrical arrangement of permanent magnets (PMs) is used to excite the fluid. The suitable distribution of magnetic field inside the MRF and the transmissible torque is obtained by moving the PMs along the axial direction. The device is designed using a magneto/mechanical FEM model, developed on purpose and based on a three-dimensional (3-D) finite-element code, which takes into account the B–H and τ–H functions of the nonlinear materials (e.g., MRF, PM, and ferromagnetic materials). The flux density maps and the shear stress maps inside the fluid are carefully analyzed. Furthermore, in order to validate the FEM model, some preliminary experimental measurements are performed on a prototype. Finally, the magnetic axial force acting on the PM system is investigated.**

***Index Terms*—FEM analysis, magnetorheological clutch, permanent magnets.**

I. Introduction

IT IS WIDELY known that magnetorheological fluids (MRFs) are able to change their rheological behavior when an external magnetic field is applied [1], [2]. They exhibit a rapid, reversible, and tunable transition from a liquid to a near-solid state as a function of the magnetic field intensity. This phenomenon is reversible and fluids can return to their liquid state in a very short time (approximately 10 ms) by removing the magnetic field [3], [4]. Typical MRF applications are found in devices used to absorb mechanical shocks and vibrations (e.g., in the automotive or aerospace industry) or in the high precision processes of polishing or finishing complex-shaped surfaces (optical lens, waveguides, hard disk, etc.) [4]–[11]. Furthermore, the MRFs have also been used to develop "haptic interfaces" capable of simulating objects in virtual environments [12]–[19]. As for magnetorheological clutches, several solutions have been proposed in the past years [20]–[30]. In all these solutions, it is a wired conventional coil that excites the fluid in order to transmit a suitable torque. However, when a fail-safe system is needed, the complexity in these devices increases as they must be provided with a continuous power supply in order to prevent a lack of electric power, which would make the coil-based clutch inoperable. As an alternative to these solutions, an exciter system, based on permanent magnets (PM), can be used. However, very few solutions using such kind of excitation have been developed in the past [31]–[40]. Although some of these devices operate quite well, some configurations present drawbacks.

For example, Johnston *et al.* [38] described a passive magnetorheological clutch. This device is mainly made of a frustum-of-cone-shaped cavity, filled with MRF, and of a PM (of the same shape) free to move along its axis. Since the axial length of the PM is smaller than the one of the cavity, when the permanent magnet is located near the cavity lower basis ("down" position), the clearance between the cavity lateral surfaces and the PM increases, resulting in a low level of field inside the MRF. On the contrary, when the PM is located near the frustum-of-cone upper basis ("up" position), the clearance is reduced and the magnetic field inside the fluid (and the transmissible torque) increases. Although the patent description gives only a few details, some peculiarities about the clutch operation can be easily deduced. First of all, the device seems to have an unsatisfactory ratio between the transmissible torque minimum and maximum value, that is, between the MRF excitation minimum and maximum levels. As a matter of fact, in the "down" position (even if the clearance increases), the PM is surrounded by the MRF, which is characterized by a relatively high level of magnetic field. Furthermore, during the clutch activation to engage the two shafts, the MRF portion around the PM is always excited, hindering the PM motion from the "down" to the "up" position and *vice versa*. This condition may result in a very poor control strategy and in an ineffective device.

In [40], the authors have explored the possibility of using a combined PM-coil exciter in order to control the magnetic field inside the fluid. The system is arranged to operate as follows: the MR clutch transmits the torque by using only the bias field of a permanent magnet that assures the fluid proper excitation (in this condition the coil is not fed). When the two shafts are disengaged, the coil is fed with a current strong enough to produce a magnetic field able to counterbalance the PM bias field, therefore obtaining a null field inside the MRF. Although this device operates in a fail-safe mode, it has two main drawbacks. The first one is that the torque limits are dictated by the coil maximum rated current capacity. Furthermore, in order not to damage the PM, the rated current value should be carefully chosen so

Manuscript received July 31, 2013; revised December 2, 2013; accepted May 12, 2014. Date of publication June 12, 2014; date of current version August 18, 2014. This work was supported by Pierburg Pump Technology Italy, S.p.A., within a framework of a project supported by Regione Toscana, P.O.R., C.R.e.O., F.E.S.R. 2007–2013. Paper no. TEC-00441-2013.

R. Rizzo and A. Musolino are with the Department of Energy and Systems Engineering, University of Pisa, Pisa 56122, Italy (e-mail: rocco.rizzo@unipi.it; musolino@dsea.unipi.it).

F. Bucchi, P. Forte, and F. Frendo are with the Department of Civil and Industrial Engineering, University of Pisa, Pisa 56122, Italy (e-mail: francesco.bucchi@for.unipi.it; p.forte@ing.unipi.it; f.frendo@ing.unipi.it).

Color versions of one or more of the figures in this paper are available online at http://ieeexplore.ieee.org.

Digital Object Identifier 10.1109/TEC.2014.2325964

that it does not outdo the permanent magnet material coercivity. The second problem is related to the quantity of electrical power needed to disengage the shafts. Since the permanent magnet has a high B_r remnant field, the magnetomotive force value produced by the coil and the electrical power related to it could reach high values, with a drastic decay of the system efficiency. The authors have tried to reduce these two drawbacks by using a clearance between the shafts of about 0.5 mm (i.e., MRF thickness). Although this thickness value does help to reduce some parameters (PM remnant field, electrical power, etc.), it seems to produce a too thin space between the shafts, creating problems in the mechanical development of the device.

This paper describes the magnetic design of an innovative fail-safe MRF clutch, obtained within the framework of a funded project, aimed to design a device capable of disengaging a power brake vacuum pump, when not needed, from a diesel engine [44].

The whole design was obtained at the end of an iterative procedure in which material choice and part assembly were driven by a joined expertise activity between researchers in mechanical and electromagnetic design.

The mechanical design and technological aspects involved in the device are reported in [41].

The device magnetic characteristics are based on an excitation system composed of PM only. The clutch actuation can be performed by axially moving the PM system, in order to obtain a given magnetic field distribution inside the MRF, in both engaged and disengaged conditions. Such arrangement allows obtaining an effective operability of the device, assuring a high level of transmissible torque when the two shafts are engaged and a near-zero torque during a disengagement condition.

This paper is organized as follows. Section II briefly describes the characteristics of the MRF, used to develop the proposed device. Section III presents a nonlinear magneto/mechanical three-dimensional (3-D) FEM model, developed on purpose and used to perform the clutch magnetic design. Section IV describes the final magnetic configuration with a detailed discussion in terms of flux density maps, shear stress maps, and transmissible torque. Section V presents some preliminary measurements, taken from a prototype, in order to experimentally validate the FEM model and to verify the effective operation of the proposed system. Finally, Section VI briefly discusses some details related to the magnetic axial force between the PMs and the ferromagnetic parts of the device; this force have to be counterbalanced in order to perform the engagement/disengagement of the proposed clutch.

II. MRF Characteristics

Several types of MRFs have been developed and commercialized in the past years. It is widely known that it is possible to describe the fluid operation by considering an MRF sample located in the gap between two plates. In absence of an applied magnetic field, the fluid may freely flow through the gap since the polarizable particles are randomly distributed in the fluid. An external magnetic field application produces a controllable yield/shear stress in the fluid that is nearly proportional to the magnitude of the magnetic field itself. Effectively, the polarizable particles within the gap align themselves along the field force lines (flux lines) creating particle chains that tend to prevent the movement of the fluid particles themselves.

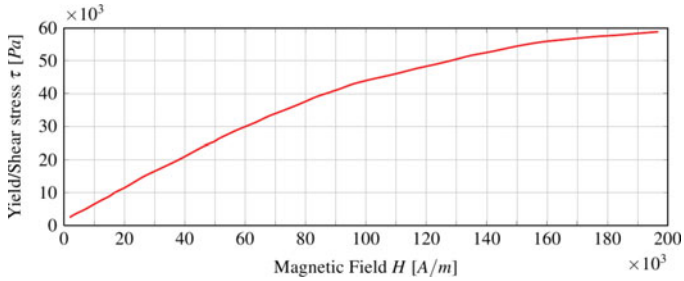

Fig. 1. Yield/shear stress τ versus magnetic field H for an MRF140CG fluid.

In our applications, we used the MRF140CG MRF produced by Lord Corporation, Cary, NC, USA [42].

Fig. 1 represents the τ–H curve of an MRF140CG at steady conditions. As far as the dynamical conditions are concerned, if the magnetic field varies from 0 to a given value H, the fluid shear/stress assumes the value expected by its characteristic curve with time delay of a few milliseconds.

The electromechanical parameter of interest is related to the yield/shear stress $\tau = \tau(H_\perp)$ that indicates the transition between a Newtonian-like and a Bingham-like behavior, that is the transition from the liquid to the semisolid state. The following equations represent the fluids simplified model, used in the simulations presented in this paper:

$$\tau < \tau_0\left(H_\perp\right) \Rightarrow \dot{\gamma} = 0 \tag{1a}$$

$$\tau = \tau_0\left(H_\perp\right) + \eta\dot{\gamma} \Rightarrow \dot{\gamma} > 0 \tag{1b}$$

where $\dot{\gamma}$ is the fluid shear rate, $\tau_0\left(H_\perp\right)$ is the yield/shear stress as a function of the magnetic field orthogonal to the transmission surfaces, and $\eta = 0.28$ Pa·s is the fluid viscosity with null magnetic field. When the fluid is excited by a proper magnetic field, if an external action produces a shear stress τ, whose value is below the material characteristic $\tau_0\left(H_\perp\right)$, the MRF keeps its semi-solid behavior and the fluid shear rate is null ($\dot{\gamma} = 0$). On the contrary, if the external action exceeds the material characteristic [$\tau \geq \tau_0\left(H_\perp\right)$], the fluid begins its transition toward a liquid state, with a fluid shear rate different from zero ($\dot{\gamma} \neq 0$); in this condition, the MRF obeys 1(b).

III. Magnetic Design

In a separate paper [41], the authors described a detailed investigation, which started from the analysis of conventional multidisk and multicylinder MRF-based clutch, allowed to derive some design criteria, useful to obtain a new improved device. As a result, a new basic clutch geometry was developed. It is shown in Fig. 2, with the design specifications. The main device components are the primary and the secondary shaft, the (sliding) PM system, and the MRF. The fluid gap can be divided into two parts. The first one, named "cylindrical part" (C), has a length L, an inner radius R_{c1},

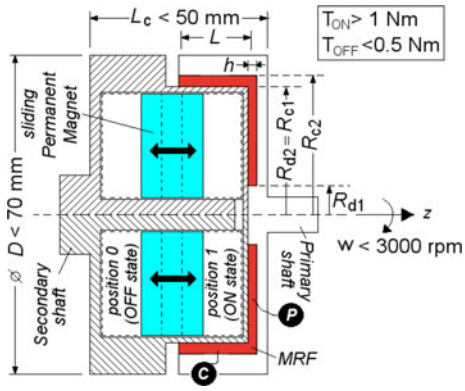

Fig. 2. Schematic view of the new basic clutch geometry with the main design specifications.

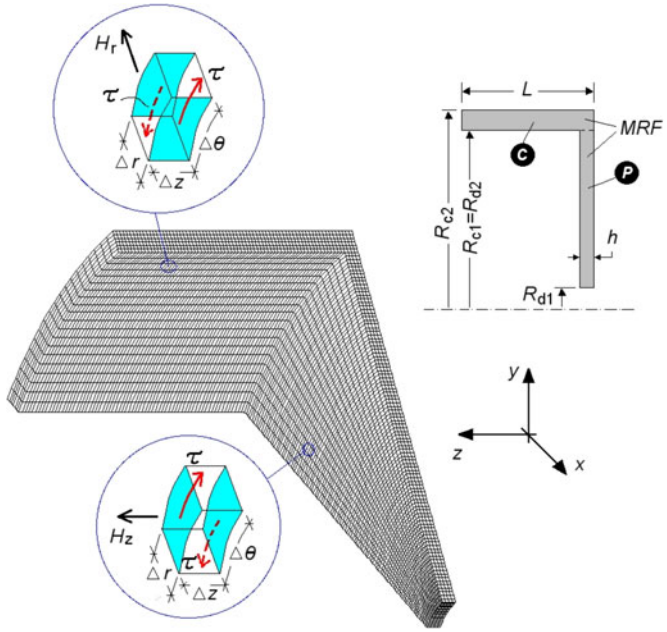

Fig. 3. 30° portion of the 3-D FE mesh fluid.

and an outer radius R_{c2}. The second part, named "planar part" (P), has an inner radius R_{d1}, an outer radius R_{d2}, and a thickness h. As described more in detail in the next sections, the device is activated by the movement of the PMs along their axial direction. When the PMs are in position 1, the fluid is excited at its maximum and the clutch is able to transmit the torque (engaged condition = ON state); on the contrary, when the PMs are in position 0, the fluid is not excited and the transmitted torque is negligibly small (disengaged condition = OFF state). Due to the specific application of the proposed MR clutch, which is the disengagement of the vacuum pump from the engine, a simple ON/OFF operation is considered. In this strategy, the PMs can be only placed in two positions (ON state or OFF state). The PM actuation is performed by the use of an external pneumatic actuator (not shown in the figures) whose feasibility analysis and detailed design are discussed in [37] and [41]. As briefly synthesized in Section C, this actuator is capable of moving the PMs from OFF to ON state (and *vice versa*), also assuring a fail-safe operating condition.

In fact, the geometry shown in Fig. 2 joins together, in a single device, the conventional disk-type and cylinder-type clutch. Furthermore, by limiting the number of disks and cylinders surfaces, this configuration allows us to retain the advantages of conventional devices, that is, the quite high transmissible torque in the engaged condition, and to reduce the drawback of the high torque in the disengaged condition due to the fluid viscosity.

However, in order to obtain an effective device, a deeper magnetic investigation should be performed. In particular, the ferromagnetic and nonferromagnetic materials arrangement around the fluid and the PM characteristics (in terms of number of poles and magnetization direction) should be carefully identified. This section describes the magnetic analysis used to design the proposed fail-safe magnetorheological clutch. Assuming the basic clutch geometry described above, the MRF gap dimensions, the PM configuration as well as the material profile were obtained at the end of an iterative procedure in which material choice and part assembly were driven by mechanical, technological, and magnetic aspects.

In order to obtain the final device, several configurations were simulated, trying to increase the ratio between the maximum and minimum torque, that is, between the transmitted torque in the engaged and disengaged conditions, while fulfilling the design requirements and constraints. The performance of the different device configurations was investigated by analyzing the magnetic flux density distribution in the MRF (produced by the PMs) and the related transmissible torque. Both these quantities were obtained by using a dedicated nonlinear numerical model based on a finite-element (FE) code [43] and described in the following.

A. Numerical Analysis

Since the behavior of MRF, the ferromagnetic iron, and the PM is highly nonlinear, an accurate investigation of the proposed system could be performed by numerical tools only. Furthermore, taking into account that some PM configurations do not allow using an axis-symmetric formulation, simulations of the device were performed using a 3-D FE model. However, since the magnetic field inside the fluid is not uniformly distributed and its direction can vary from point to point, the code was integrated with a dedicated tool capable of numerically calculating the transmissible torque, exploiting the same FE mesh used for the magnetic analysis.

Fig. 3 shows a 30°-portion of the 3-D mesh used to develop the magneto/mechanical complete model. The MRF τ–H curve (see Fig. 1) was used to obtain the shear stress value $\tau(H_\perp)$ for each elementary volume of the mesh. Then, the transmissible torque was calculated by integrating the elementary contributions over the whole volume occupied by the fluid.

In the "cylindrical" part (C), the torque developed by a single fluid volume element, centered in r, is

$$\Delta T_c = \tau(H_r) r^2 \Delta\theta \Delta z. \tag{2}$$

The shear rate $\dot{\gamma}$ can be expressed in terms of the rotation speed ω_r in the fluid at radius r

$$\dot{\gamma} = r\frac{d\omega_r}{dr}. \tag{3}$$

Handling (1b)–(3), the ω_r differential can be obtained as follows:

$$d\omega_r = \frac{\dot{\gamma}}{r}\cdot dr = \frac{1}{\eta}\left[\frac{\Delta T_c}{r^3\Delta\theta\Delta z} - \frac{\tau_0(H_r)}{r}\right]dr. \tag{4}$$

Assuming that the mesh is small enough, the term $\Delta T_c/\Delta\theta\Delta z$ inside the volume element can be assumed as constant, and (4) can be integrated applying the boundary conditions, $\omega_r = \Omega_1$ at $r = R_{c1}$ and $\omega_r = \Omega_2$ at $r = R_{c2}$. The elementary transmissible torque is

$$\Delta T_c = \frac{2R_{c1}^2R_{c2}^2}{R_{c2}^2 - R_{c1}^2}\cdot\left[\eta\Delta\Omega + \int_{R_{c1}}^{R_{c2}}\frac{\tau_0(H_r)}{r}\cdot dr\right]\cdot\Delta\theta\Delta z \tag{5}$$

where $\Delta\Omega = \Omega_2 - \Omega_1$ is the mechanical slip between the primary and secondary shafts.

Finally, the torque developed by the MRF "cylindrical" part is obtained by integrating (5) over the fluid inner lateral surface

$$T_c = \int_0^{2\pi}\int_0^L dT_c\cdot d\theta dz = \frac{2R_{c1}^2R_{c2}^2}{R_{c2}^2 - R_{c1}^2}\cdot\left[\eta\Delta\Omega 2\pi L + \int_{R_{c1}}^{R_{c2}}\int_0^{2\pi}\int_0^L\frac{\tau_0(H_r)}{r}\cdot dr d\theta dz\right] \tag{6}$$

where the first term on the right-hand side of the equation is the torque viscous component, while the second term is the magnetic-field-dependent component. However, since the magnetic field inside the fluid is not uniformly distributed and its direction can vary from point to point, the volume integral appearing in the latter torque component can be numerically solved exploiting the same FE mesh used for the magnetic analysis.

As for the (P) part, a similar approach can be used. In this case, the torque developed by a single fluid volume element is $\Delta T_p = \tau(H_z)r^2\Delta r\Delta\theta$, while the shear rate becomes $\dot{\gamma} = r\frac{d\omega_r}{dz}$. As a consequence, the ω_r differential is

$$d\omega_r = \frac{\dot{\gamma}}{r}\cdot dz = \frac{1}{\eta}\left[\frac{\Delta T_p}{r^3\Delta r\Delta\theta} - \frac{\tau_0(H_z)}{r}\right]dz. \tag{7}$$

By integrating (7) along the z-direction and applying the boundary conditions: $\omega_r = \Omega_1$ at $z = h$ and $\omega_r = \Omega_2$ at $z = 0$, the elementary transmissible torque becomes

$$\Delta T_p = \frac{1}{h}\left[\eta\Delta\Omega\cdot r^3 + \int_0^h\tau_0(H_z)\cdot r^2\cdot dz\right]\cdot\Delta r\Delta\theta. \tag{8}$$

The torque developed by the MRF "planar" part is obtained by integrating (8) over the fluid basis surface

$$T_p = \int_{R_{d1}}^{R_{d2}}\int_0^{2\pi} dT_p\cdot dr d\theta = \frac{1}{h}\left[\frac{\eta\Delta\Omega\pi}{2}\left(R_{d2}^4 - R_{d1}^4\right) + \int_{R_{d1}}^{R_{d2}}\int_0^{2\pi}\int_0^L\tau_0(H_z)r^2\cdot dr d\theta dz\right] \tag{9}$$

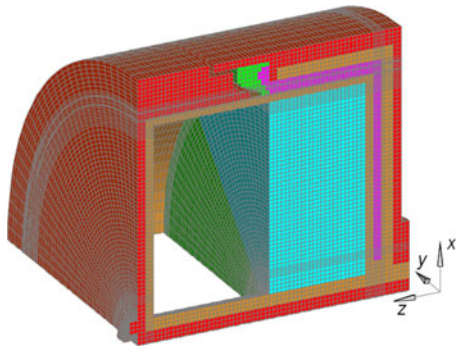

Fig. 4. FE model of the device.

where the first term on the right-hand side of the equation is the torque viscous component, while the second term is the magnetic-field-dependent component.

Also in this case, the volume integral appearing in the right-hand side of (9) can be evaluated numerically.

Finally, the total torque transmissible by the clutch is the sum of the two terms calculated by using (6) and (9)

$$T = T_c + T_p. \tag{10}$$

B. Simulation Results

Because of the problem symmetries, only one quarter of the whole structure can be analyzed, resulting in a reduced complexity of the 3-D magnetostatic FE model. The results obtained by the nonlinear magnetostatic model are also valid in the presence of a slip between the two axes if the currents induced by motional effects can be neglected (as done in this paper). The FE mesh, shown in Fig. 4, contains about 1×10^6 elements and takes about 40 min of CPU time on a Linux machine with 24 GB of RAM.

As an example, Fig. 5(a) and (b) shows the magnetic flux density maps in the MRF, with two different distributions and profiles of ferromagnetic and nonferromagnetic material around the fluid gap, when the PM system (radially magnetized) is in the ON state.

Fig. 6(a) and (b) shows the magnetic flux density B along the lines $A - A'$ and $B - B'$ through the MRF, respectively, in the (C) and (P) parts, for the two different configurations shown in Fig. 5. The results show that in the device arranged with the configuration 2, even though the field B along the line $A - A'$ slightly decreases, it considerably increases along the line $B - B'$, allowing better performance with respect to the configuration 1 (see also Fig. 13).

Besides the materials profile, the numerical simulations allowed also to design the excitation system, which is based on rare-earth PM. The poles number and the magnetization type were chosen in order to transmit as high as possible torque within the given geometry. Furthermore, the PM system was defined taking into account the magnetic configuration feasibility with respect to the device dimensions and to the reduction of the axial magnetic force. Fig. 7 shows the magnetic flux density B inside the fluid along the azimuthal direction in the (C) part

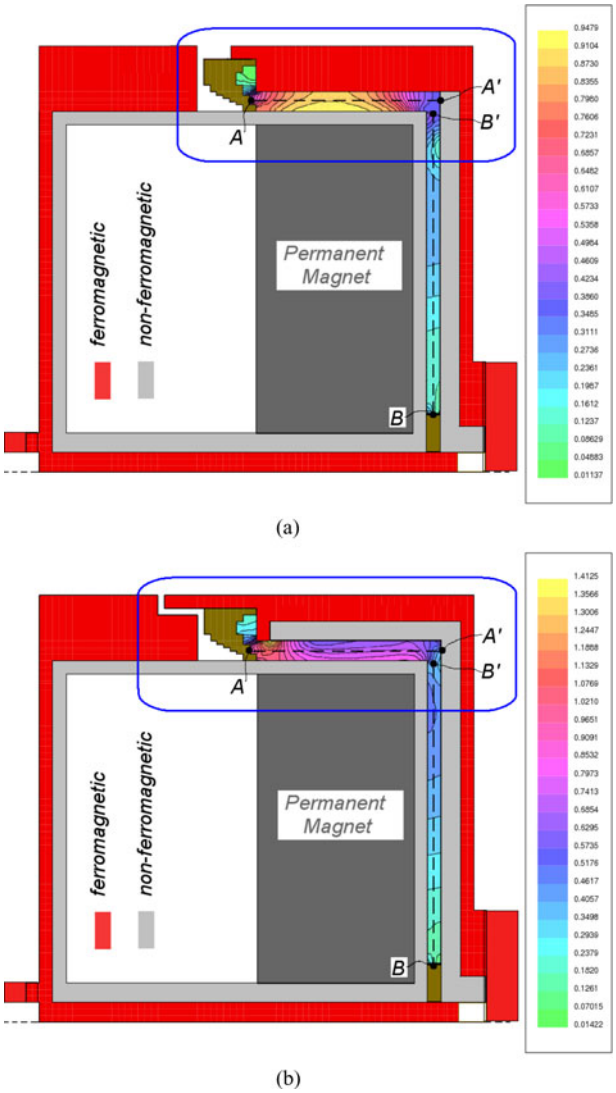

Fig. 5. Magnetic flux density map inside the MFR for two different materials profile configurations. (a) Configuration 1. (b) Configuration 2.

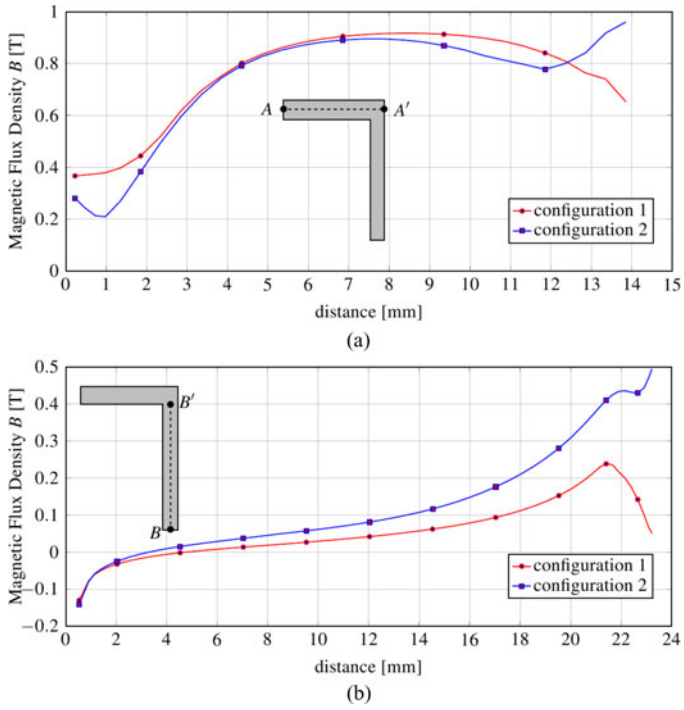

Fig. 6. Comparison of B for the two configurations shown in Fig. 5. (a) Radial component of B along the Line $A - A'$. (b) Axial component of B along the Line $B - B'$.

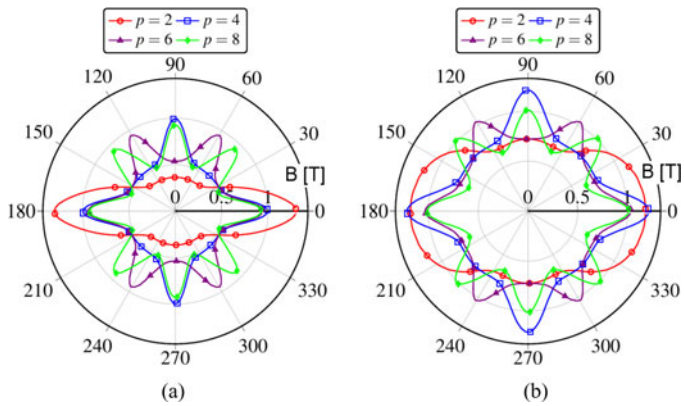

Fig. 7. Comparison of the field B for two different PM system configurations. (a) Radial PM. (b) Diametral PM.

center for two different PM system configurations. In particular, for a given device geometry, the field B was analyzed modifying the number of poles p (from 2 to 8) and the PM magnetization type (R = radial and D = diametral). The results show that the highest MRF excitation level is obtained by using a PM system, composed of four 90°-poles, alternately magnetized along their diametral direction, as shown in Fig. 8.

For the sake of brevity, we do not describe simulations and results concerning the device with the exciter system in the OFF state. However, at the end of the synthesis procedure, a final device configuration is defined. It will be described and further analyzed in the next section.

IV. Final Magnetic Configuration

The final magnetic configuration with its main dimensions is shown in Fig. 9(a). As for the device materials, the primary shaft dark blue piece and secondary shaft dark green piece

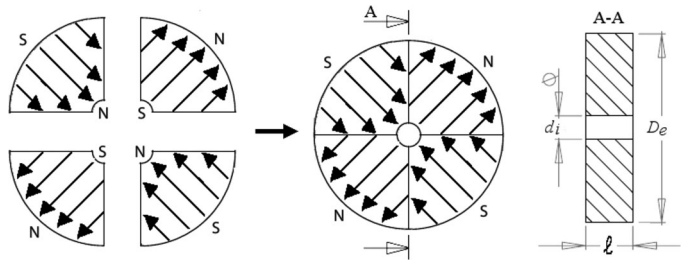

Fig. 8. Schematic view of the PM system with magnetization directions.

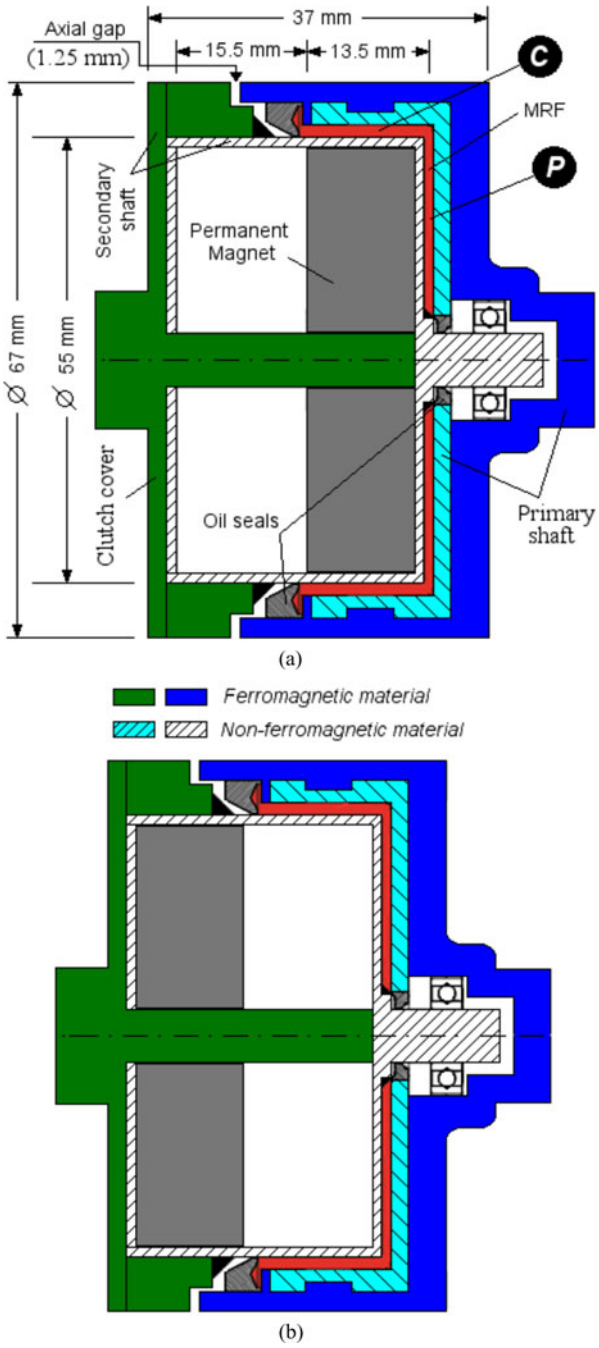

Fig. 9. Schematic view of the proposed device and its operation. (a) ON state (engaged shafts). (b) OFF state (disengaged shafts).

are made of ferromagnetic iron AISI-1018. On the contrary, the dashed light blue and the dashed white parts are made of nonferromagnetic iron AISI-316L. The PM system is a hollow cylinder, composed of four NdFeB 90°-sectors, diametrally magnetized (see Fig. 8), whose characteristics and dimensions are reported in Table I.

A. Device Operation

From a magnetic point of view, the system operates as follows. Let us assume that the clutch is initially at rest with primary and secondary shafts disengaged. This condition is ensured by the fact that the PM is far enough from the MRF so that the magnetic field does not excite the fluid [OFF state, Fig. 9(b)]. Once the decision to transmit the torque between the two shafts has been taken, the PM must be activated moving it along its axis direction. During the PM movement, as the distance between the magnet itself and the fluid is reduced, the magnetic field inside the MRF increases, and consequently so does the transmitted torque. As soon as this torque exceeds the load on the secondary shaft, it begins to rotate. The highest field and torque values are obtained when the permanent magnet is surrounded by the MRF [ON state, Fig. 9(a)].

TABLE I
PM EXCITER SYSTEM CHARACTERISTICS AND MAIN DIMENSIONS

Material	Physical Characteristics	Dimensions [mm]
NdFeB	$B_r = 1.36\ T$; $H_c = 10.2 \times 10^5\,\mathrm{A/m}$; $T_{\max} = 150°\mathrm{C}$;	$D_e = 52.8\mathrm{mm}(\pm 0.05)$; $d_i = 6.2\mathrm{mm}(\pm 0.05)$; $\ell = 12\mathrm{mm}(\pm 0.05)$;

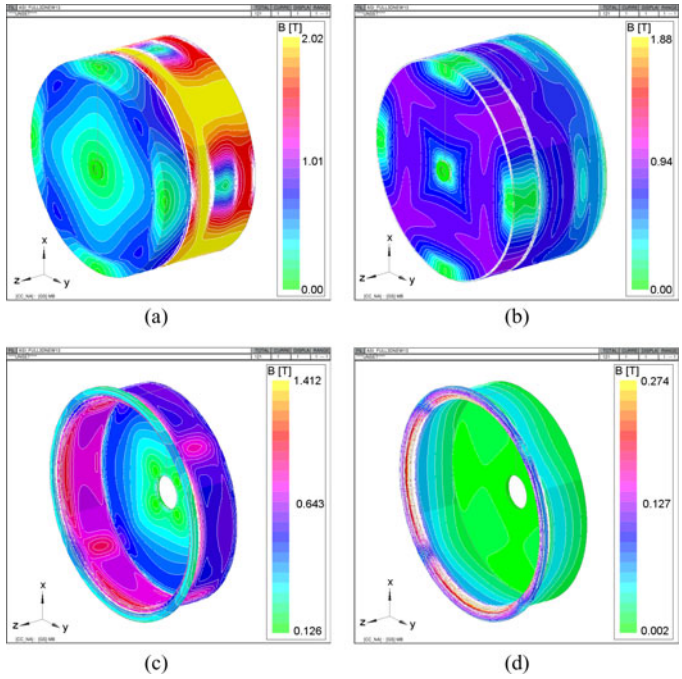

Fig. 10. Flux density maps B in the ON and OFF state. (a) 3-D view of the device (ON state). (b) 3-D view of the device (OFF state). (c) 3D view of the MRF (ON state). (d) 3D view of the MRF (OFF state).

B. Performance Evaluation

Fig. 10(a) and (b) shows the maps of magnetic flux density B on the clutch external surface, when the PM are in the ON and OFF states, respectively. Fig. 10(c) and (d) shows the field maps in the fluid only, in the same conditions as the previous figures. As for the mechanical characteristic, Fig. 11 shows the shear stress maps in the MRF corresponding to the field conditions reported in Fig. 10(c) and (d). From these results, it follows that in the ON state, the magnetic flux density is high enough to

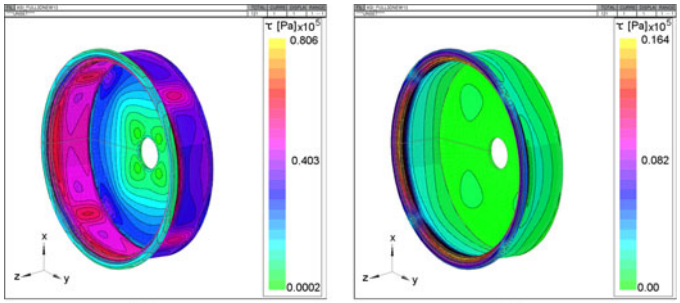

Fig. 11. Shear stress maps τ inside the MRF. (a) ON state. (b) OFF state.

result in a high shear stress and consequently in a high level of transmissible torque between the primary and secondary shafts. On the contrary, the OFF state is characterized by very low magnetic flux density and shear stress, resulting in a condition of disengaged shafts.

C. Calculated Torque

The torque transmissible by the proposed clutch has been calculated by using the mathematical model described in Section III-A. Fig. 12 shows the magnetic flux density in the MRF on a cut of the 3-D clutch model $x-z$ plane at $y=0$, as a function of the PM displacement. The sequence of the four figures shows an increasing field in the fluid when the permanent magnet is pushed from the OFF to the ON state, so performing the engagement of the clutch. The same figure shows the torque values (due to the MRF only) as a function of the permanent magnet displacement during its (quasi-static) motion between the OFF and ON states. Simulations results were obtained working on a relative mechanical speed of 1200 r/min between the primary and secondary shafts. From the results, it follows that the system is able to transmit a maximum torque of about 3 N·m (ON state), while the minimum torque (in the OFF state) is about 0.18 N·m. The latter value is the sum of approximately 0.082 N·m viscous components and of the torque components due to the magnetic field residual value inside the fluid.

As for the contribution to the torque, ascribable separately to the (C)-part and (P)-part, Fig. 13 shows the vectors of the magnetic induction B inside the fluid. The (P)-part (in the upper side) is excited by a magnetic induction B whose main component is orthogonal to the transmission surfaces. Numerically, referring to the torque in the ON state ($T_z = 3$ N·m), the (P)-part contributes for about 15% and the (C)-part for about 85%.

V. Experimental Measurements

In order to validate the FEM model, preliminary magnetic measurements were carried out on a prototype of the designed clutch. Fig. 14 shows some pictures of the prototype, where it is possible to clearly distinguish the PM and the chamber in which they move.

At first, the device has been analyzed from a magnetic point of view, comparing the simulated magnetic field with the one measured. Since it is quite difficult to measure the magnetic field

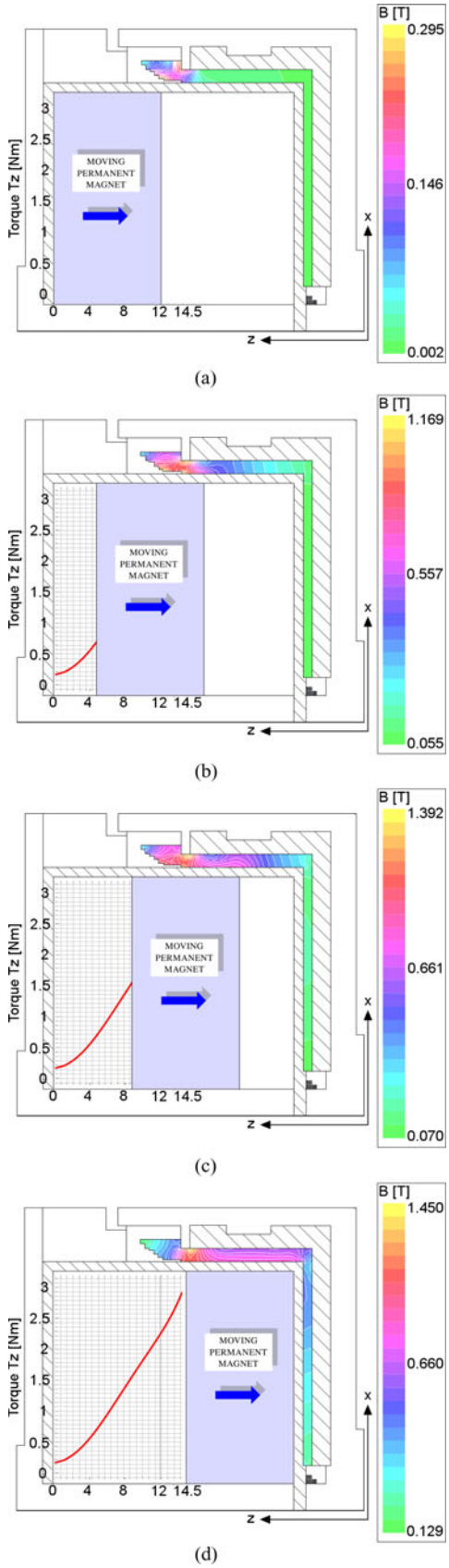

Fig. 12. Flux density maps inside the MRF as a function of PM displacement. (a) OFF state: $Tz = 0.18$ N·m. (b) $\Delta z = 4.8$ mm: $Tz = 0.70$ N·m. (c) $\Delta z = 8.9$ mm: $Tz = 1.64$ N·m. (d) ON state: $Tz = 2.98$ N·m.

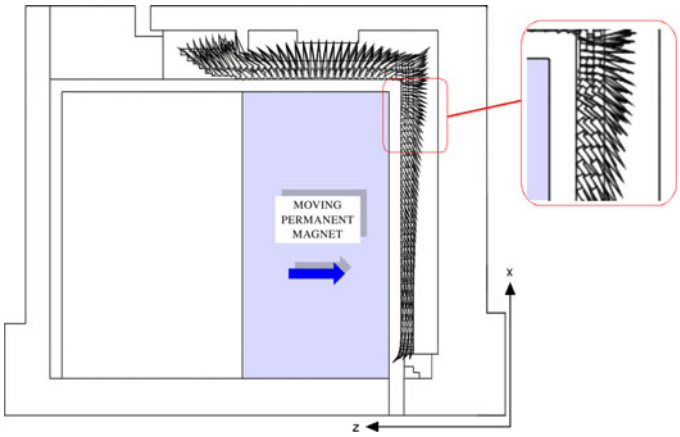

Fig. 13. Magnetic induction vectors inside the MRF.

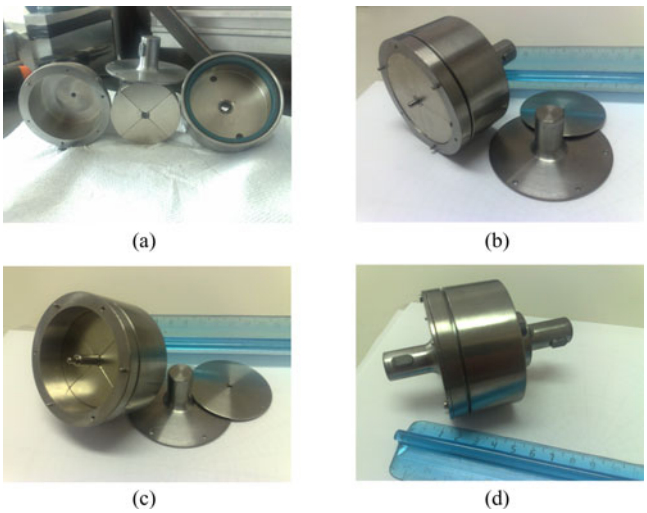

Fig. 14. Preliminary clutch prototype. (a) System components. (b) OFF state. (c) ON state. (d) Assembled clutch.

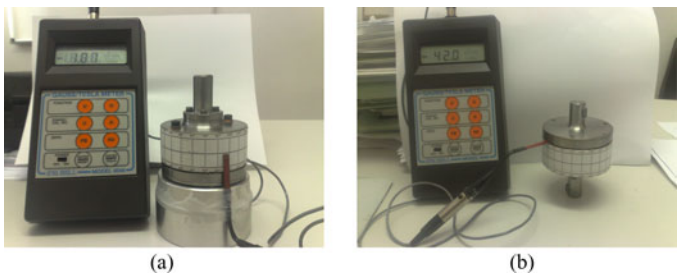

Fig. 15. Experimental setup to measure the flux density B. (a) Radial field measurements. (b) Axial field measurements.

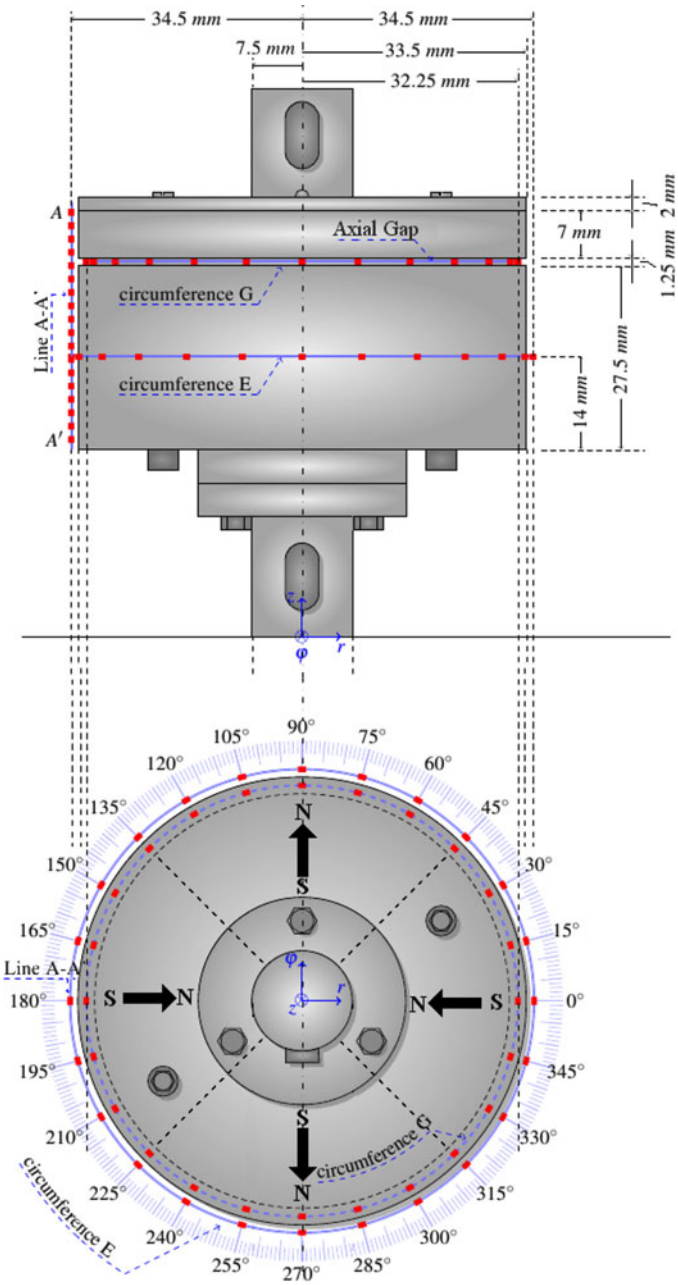

Fig. 16. Measurement points (in red) of flux density B.

inside the MRF without altering the flux lines, the validation of the FEM model was carried out referring to the free space. Measurements have been performed by using a portable Gauss-meter F.W. Bell/4048 (see Fig. 15) equipped with an accurate Hall sensor.

As shown in Fig. 16, the magnetic field (both axial and radial component) was measured every 7.5° along the E and G Circumferences and along an axis direction (Line A–A'), with the PMs in the ON State. Fig. 17 show the results of these comparisons.

In the case of Fig. 17(a), the maximum error is less than 8%. The agreement between measured and simulated quantities is fully satisfactory because of unavoidable errors in measuring (instrument calibration, imprecise probe positioning, etc.) and the FEM modeling. Furthermore, other inaccuracies may be introduced by using the AISI-1018 nonlinear ferromagnetic *B–H* curve as the average between several ones found in the literature, as well as by using the MRF *B–H* curve.

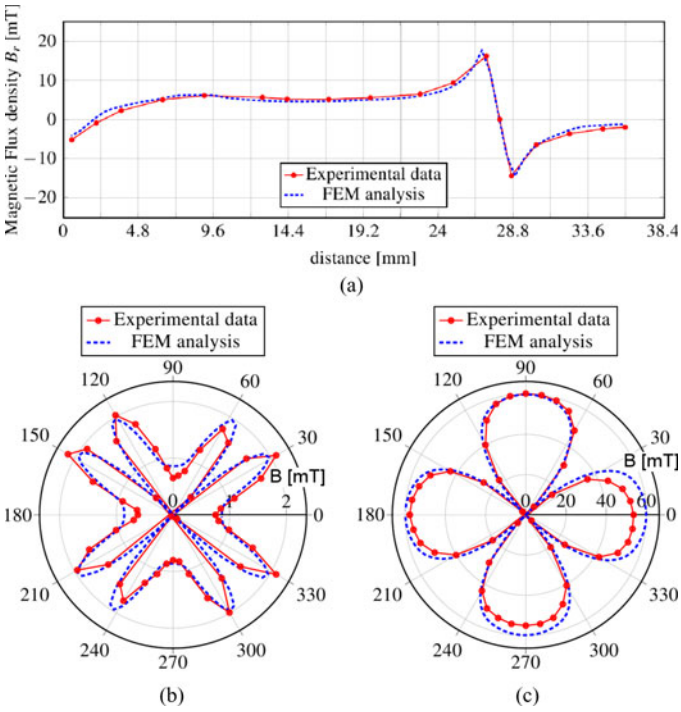

Fig. 17. Comparison between simulated and measured flux density B in the measurement points shown in Fig. 16. (a) B_r along line A–A'. (b) B_z along circumference E. (c) B_z along circumference G.

As for the comparisons carried out along the E and G circumferences (see Fig. 16), a minor lack of axial gap uniformity was detected during the measurement activity.

In fact the axial gap, in a circumferential extension of about $240°$, turns out to be slightly wider than in the remaining $120°$. Such anomaly, in the order of 0.1–0.2 mm, is also reflected in the difference between experimental and FEM theoretical model values, where the gap is constant along the entire circumference. In both cases, the maximum errors fall exactly in the areas where the gap deviates from its nominal value (1.25 mm).

However, in order to verify the influence of the axial gap uncertainty on the MRF excitation level, some simulations varying the gap distance of about $\pm 20\%$ were also performed. Fig. 18(a) and (b) shows the flux density modulus inside the fluid along the azimuthal direction in the (C) part center both for the ON and OFF states.

The comparison shows that when the system is in both ON and OFF states, the magnetic field inside the fluid is substantially indifferent to the small variations of the axial gap, which are responsible for relatively large variation of the magnetic flux density outside the device.

On the contrary, as shown in Fig. 18(c) and (d), when the PM is positioned at the intermediate points between the OFF and ON states, any change in the gap thickness modifies the magnetic field in the MRF. This behavior must be taken into account in a subsequent design phase in order to reduce the system sensitivity by changes in the mechanical tolerances.

In order to investigate the effective device operation, an experimental mechanical setup was developed. The design and realization of this setup as well as a deeper analysis of the mechanical tests on the clutch prototype are described in [41]. Here,

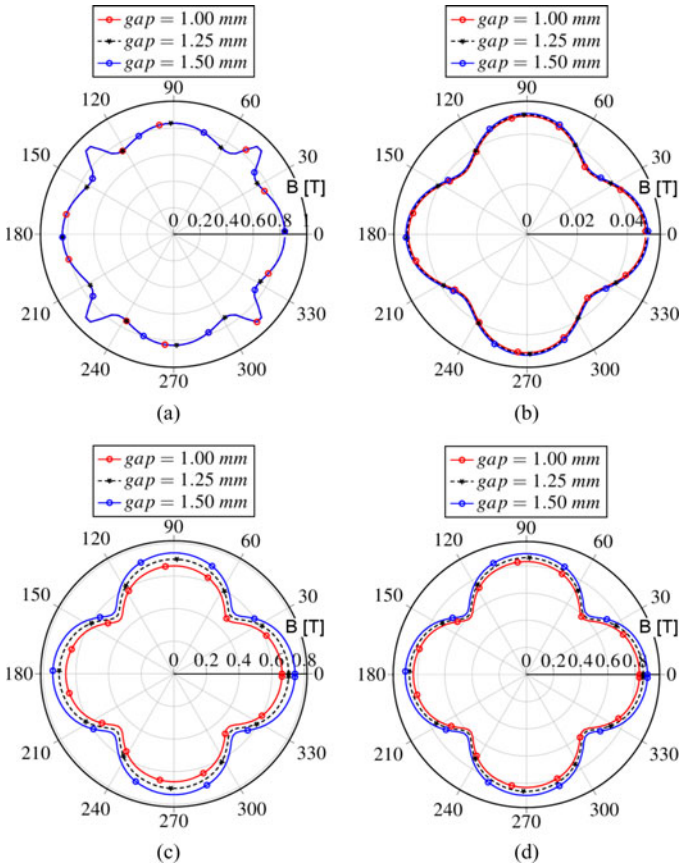

Fig. 18. Flux density modulus inside the fluid along an azimuthal direction in the C part center as a function of the axial gap thickness, for different values of PM displacement. (a) ON state: max err. $= 0.009\%$. (b) OFF state: max err. = 1.2%. (c) $\Delta z = 8.5$ mm: max err. $= 10\%$. (d) $\Delta z = 11$ mm: max err. = 5.5%.

only some preliminary tests are reported in order to validate the FEM model.

By using the magneto/mechanical model described in Section III-A, the transmissible torque value, as a function of the PM displacement was calculated. Simulations were performed with a relative mechanical speed of $\Delta\Omega = 1200$ r/min between the primary and secondary shafts. Fig. 19 shows the comparison between the simulation results and the experimental data, cleaned from the parasitic torque (bearings, oil seals, etc.). It appears that simulated and measured torque values match quite well in the ON and OFF states. On the contrary, when the PM is in intermediate positions, relatively large errors are found due to the axial gap uncertainty previously discussed.

This analysis shows that the agreement between measured and simulated quantities is fully satisfactory, and therefore, the developed FEM model is able to predict the device operation with acceptable errors.

VI. Magnetic Axial Force

A. *OFF ⇔ ON Magnetic Force*

Besides the parasitic frictions (bearings, oil seals, etc.), there is also a magnetic force acting in the axial direction that may either hinders or facilitates the PM motion from the OFF state

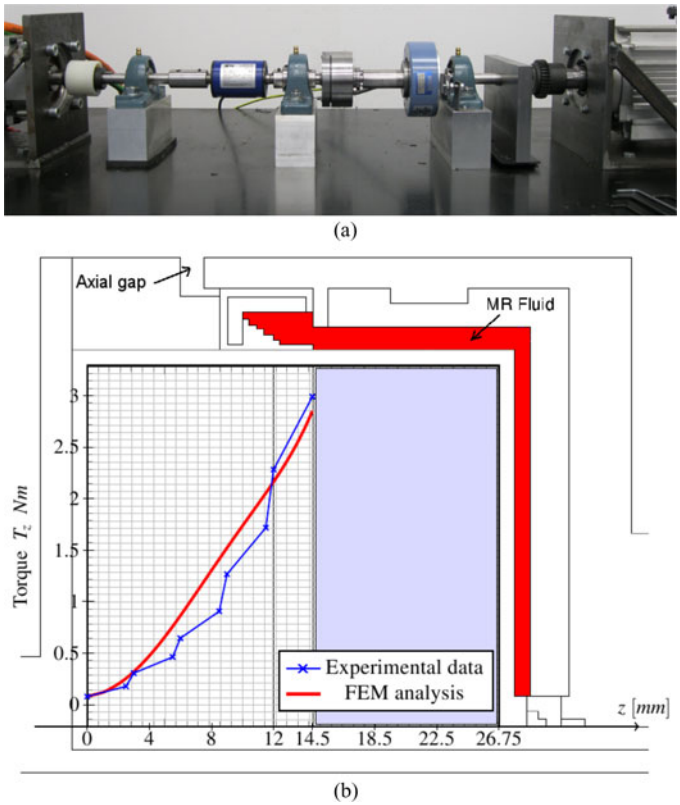

Fig. 19. Test bench and comparison between simulated and measured transmissible torque as a function of the PM displacement. (a) Test bench. (b) Comparison.

to the ON state and *vice versa*. This force is due to the natural attractive behavior between PMs and ferromagnetic materials. Fig. 20 shows the axial magnetic force profile as a function of the PM displacement.

Given the above, it seems clear that this force tends to keep the PM in its position when it stays in both OFF or ON positions (stable positions). PM intermediate displacements, instead, are characterized by a profile that strongly depends on the ferromagnetic material distribution around the clutch central zone. Nevertheless, the magnetic force values in these intermediate points are always negative, tending to bring the PM to the OFF state.

B. Preliminary Experimental Evaluation of the Magnetic Force

As a very preliminary evaluation of the magnetic axial force, a rough but effective experimental setup was developed. As shown in Fig. 21(a), it consists of an aluminum cylinder (of about 240 g), with the same radius as the PM, and of a set of calibrated weights. The clutch was deprived of the top cover and the aluminum cylinder was gradually loaded with increasing weights, so measuring the lowering of the cylinder. Fig. 21(b) reports the comparison between experimental and simulated data, showing a fully satisfactory agreement between them.

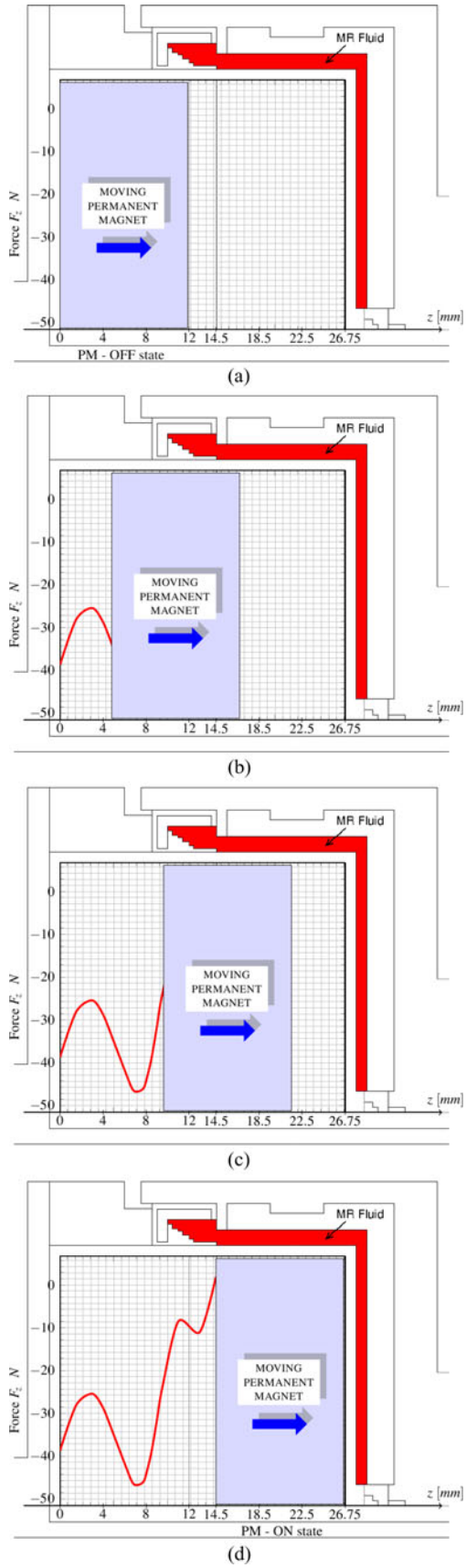

Fig. 20. Magnetic axial force as a function of the PM displacement. (a) OFF state: $F_z = -38.7$ N. (b) $\Delta z = 4.8$ mm: $F_z = -34$ N. (c) $\Delta z = 9.6$ mm: $F_z = -22.3$ N. (d) ON state: $F_z = +2$ N.

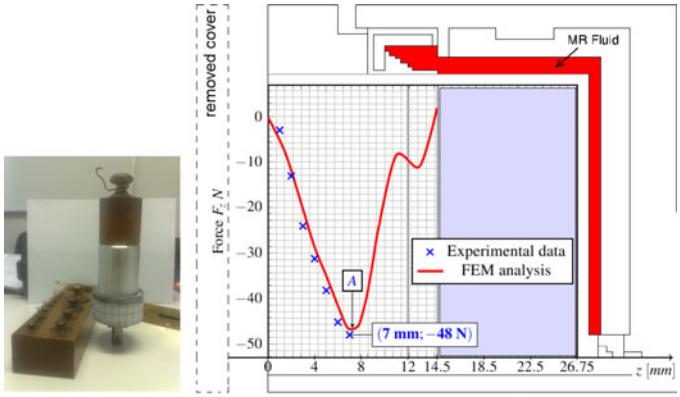

Fig. 21. Preliminary verification of the magnetic axial force. (a) Experimental setup. (b) Comparison.

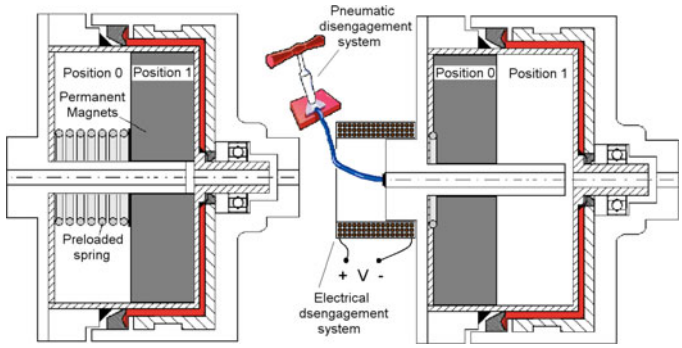

Fig. 22. Schematic view of a clutch engagement/disengagement system.

At low values of z, the force profile in the Fig. 21(b) differs from that of Fig. 20(d) because the former has been obtained in the absence of the ferromagnetic cover, which has been removed to perform the practical measurements.

However, since the A point represents an unstable position, the used experimental method can only verify the left side of the force profile.

C. Device Control and PM Actuation

The magnetic axial force added with the parasitic frictions have to be counterbalanced in order to perform the engagement/disengagement of the proposed clutch. In the ON/OFF operation strategy, used for the specific application, the PM movement is obtained by a pneumatic actuator, which uses the vacuum pump itself to impose a proper pressure force, capable to move the PM system along its axis direction. This solution was proved to be effective and reliable in [37] and [41].

However, more complex operation strategies could be envisaged to perform the device actuation. They could be based on the *position* strategy, in which the torque value can be controlled by moving, step by step, the PM along its axis direction, increasing or decreasing the magnetic field inside the fluid. In this case, a fine control can be obtained by means of electrical actuators (e.g., electrical solenoids, linear stepper motors, and so forth).

Whatever strategy and actuator is used, a fail-safe operating condition must be assured. In the case of external failure, the device have to transmit the torque between the two shafts, that is, the PM system should be normally positioned in the ON state. As a consequence, the scheme shown in Fig. 22 can be followed: The engagement phase (moving the PMs from position 0 to position 1) is assured by a preloaded spring; the disengagement phase can be obtained by the use of an external (pneumatic or electrical) actuator, which moves the system back to position 0.

Defaults in the fail-safe characteristic of the proposed device are possible if the spring breaks (usually a very uncommon event). In particular, observing the values of the magnetic axial force [see Fig. 20(d)], failure occurs only if the spring breaks when the PMs are in the OFF state. In this condition, the magnetic axial force keeps the PMs in their (OFF) position. Anyhow, in the case of spring failure, if a pneumatic actuator is used, its operation can be properly inverted, allowing to push the PM system in the ON state, where the positive magnetic force tends to keep them.

VII. Conclusion

In this paper, the magnetic design and the experimental validation of a clutch, based on MRF, were described. The MRF gap geometry, the PM configuration as well as the proper distribution of ferromagnetic and nonferromagnetic materials around the fluid were obtained by means of a 3-D magneto/mechanical FE code capable of taking into account all clutch magnetic features. The result of this research activity was the development of an innovative, effective, and fail-safe MRF-based clutch.

The main innovation of the proposed device relies in the use of a system of PM to excite the MRF. This excitation system has some advantages with respect to similar devices based on the use of systems of coils [45]: 1) intrinsic fail-safe operation; and 2) increased transmissible torque with the same size. This is due to the use of PMs, instead of the space-consuming coils, in order to obtain the proper excitation magnetic field.

On the contrary, the coil-based MRF clutches are easier to control when a continuous varying transmissible torque is required.

References

[1] J. D. Carlson, "The promise of controllable fluids, " in *Proc. Actuator*, Bremen, Germany, 1994, pp. 266–270.
[2] J. D. Carlson, D. N. Catanzarite, and K. A. St. Clair, "Commercial magneto-rheological fluid device," in *Proc. 5th Int. Conf. ER Fluids, MR Suspensions Associated Technol.*, 1996, pp. 20–28.
[3] C. W. Macosko, *Rheology: Principles, Measurements, and Applications*. New York, NY, USA: VCH, 1994.
[4] W. I. Kordonsky, "Elements and devices based on magnetorheological effect," *J. Intell. Mater. Syst. Struct.*, vol. 4, no. 1, pp. 65–69, 1993.
[5] W. I. Kordonsky, "Magnetorheological effect as a base of new devices and technologies," *J. Magn. Magn. Mater.*, vol. 122, no. 1–3, pp. 395–398, 1993.
[6] X. Zhu, X. Jing, and L. Cheng, "Magnetorheological fluid dampers: A review on structure design and analysis," *J. Intell. Mater. Syst. Struct.*, vol. 23, pp. 839–873, 2012.
[7] T. Kikuchi, K. Kobayashi, and A. Inoue, "Gap-Size effect of compact MR fluid brake," *J. Intell. Mater. Syst. Struct.*, vol. 22, pp. 1677–1683, 2011.
[8] A. Shorey and M. DeMarco, "Application of magneto-rheological finishing (MRF) to the figuring of adaptive optics systems," presented at the Adapt. Opt.: Methods, Anal. Appl., Charlotte, NC, USA, Jun. 6, 2005.

[9] G. Bossis and E. Lemaire, "Yield stresses in magnetic suspensions," *J. Rheol.*, vol 35, no. 7, pp. 1345–1354, 1991.
[10] W. Kordonsky, O. Ashour, and C. A. Rogers, "Magnetorheological fluids: Materials, characterization, and devices," *J. Intell. Mater. Syst. Struct.*, vol. 7, pp. 123–130, 1996.
[11] A. G. Olabi and A. Grunwald, "Design and application of magnetorheological fluid," *Mater. Des.*, vol. 28, pp. 2658–2664, 2007.
[12] J. D. Carlson, "Portable hand and wrist rehabilitation device," U.S. Patent 6117 093, Sep. 12, 2000.
[13] B. Liu, W. H. Li, P. B. Kosasih, and X. Z. Zhang, "Development of an MR-brake-based haptic device," *Smart Mater. Struct.*, vol. 15, pp. 1960–1966, 2006.
[14] E. P. Scilingo, N. Sgambelluri, D. De Rossi, and A. Bicchi, "Haptic displays based on magnetorheological fluids: Design, realization and psychophysical validation," in *Proc. 11th Symp. Haptic Interfaces Virtual Environ. Teleoperator Syst.*, 2003, pp.10–15.
[15] M. Avraam, M. Horodinca, I. Romanescu, and A. Preumont, "Computer controlled rotational MR-brake for wrist rehabilitation device," *J. Intell. Mater. Syst. Struct.*, vol. 21, pp. 1543–1557, Oct. 2010.
[16] A. Bicchi, M. Raugi, R. Rizzo, and N. Sgambelluri, "Analysis and design of an electromagnetic system for the characterization of magnetorheological fluids for haptic interfaces," *IEEE Trans. Magn.*, vol. 41, no. 5, pp. 1876–1879, May 2005.
[17] R. Rizzo, N. Sgambelluri, E. P. Scilingo, M. Raugi, and A. Bicchi, "Electromagnetic modeling and design of haptic interface prototypes based on magnetorheological fluids," *IEEE Trans. Magn.*, vol. 43, no. 9, pp. 3586–3598, Sep. 2007.
[18] R. Rizzo, "A permanent magnets exciter for MRF-based haptic interfaces," *IEEE Trans. Magn.*, vol. 49, no. 4, pp. 1390–1401, Apr. 2013.
[19] N. Sgambelluri, E. P. Scilingo, A. Bicchi, R. Rizzo, and M. Raugi, "Advanced modelling and preliminary psychophysical experiments for a free-hand haptic device," in *Proc. IEEE/RSJ Int. Conf. Intell. Robots Syst.*, 2006, pp.1558–1563.
[20] J. Rabinow, "The magnetic fluid clutch," *Trans. Amer. Inst. Elect. Eng.*, vol. 67, no. 2, pp. 1308–1315, 1948.
[21] D. Guth, D. Cording, and J. Maas, "MRF based clutch with integrated electrical drive," in *Proc. IEEE/ASME Int. Conf. Adv. Intell. Mechatron.*, Jul. 3–7, 2011, pp. 493–498.
[22] A. M. Clemente, A. F. Caballero, D. B. Rojas, D. Copaci, and L. M. Lorente, "Elbow functional compensation using a lightweight magnetorheological clutch," in *Proc. IEEE Annu. Int. Conf. Eng. Med. Biol. Soc.,* Aug. 30–Sep. 3, 2011, pp. 5215–5218.
[23] H. Y. Fu, T. Z. Zhi, and W. N. Nan, "Numerical calculation of torque transmission and magnetic circuit finite element analysis of a magnetorheological clutch," in *Proc. Int. Conf. Comput., Control Ind. Eng.*, Jun. 5–6, 2010, vol. 1, pp. 403–407.
[24] Z. S. Fei and L. Yong, "Disc shaped high-torque-MRF-clutch design," in *Proc. Int. Conf. Comput. Appl. Syst. Model.*, Oct. 22–24, 2010, vol. 13, pp. V13-374–V13-377.
[25] U. Lee, D. Kim, N. Hur, and D. Jeon, "Design analysis and experimental evaluation of an MR fluid clutch," *J. Intell. Mater. Syst. Struct.*, vol. 10, no. 9, pp. 701–707, 2000.
[26] B. Kavlicoglu, F. Gordaninejad, C. A. Evrensel, N. Cobanoglu, Y. Liu, and A. Fuchs, "A high-torque magnetorheological fluid clutch," in *Proc. SPIE Conf. Smart Mater. Struct.*, 2002, pp. 393–400.
[27] E.-S. Kim, S.-B. Choi, Y.-G. Park, and S. Lee, "Temperature control of an automotive engine cooling system utilizing a magnetorheological fan clutch," *Smart Mater. Struct.*, vol. 19, no. 10, pp. 1–10, 2010.
[28] J. Z. Chen and W. H. Liao, "Design, testing and control of a magnetorheological actuator for assistive knee braces," *Smart Mater. Struct.*, vol. 19, no. 3, pp. 1–10, 2010.
[29] B. M. Kavlicoglu, F. Gordaninejad, C. A. Evrensel, Y. Liu, N. Kavlicoglu, and A. Fuchs, "Heating of a high-torque magnetorheological fluid limited slip differential clutch," *J. Intell. Mater. Syst. Struct.*, vol. 19, pp. 235–241, Feb. 2008.
[30] T. Kikuchi, K. Ikeda, K. Otsuki, T. Kakehashi, and J. Furusco, "Compact MR fluid clutch device for human-friendly actuator," in *Proc. 11th Conf. Electrorheological Fluids Magnetorheological Suspensions*, vol. 149, no. 012059, 2009, p. 4.
[31] H. Böse, J. Ehrlich, and A.-M. Trendler, "Performance of magnetorheological fluids in a novel damper with excellent fail-safe behavior," in *Proc. 11th Conf. Electrorheological Fluids Magnetorheological Suspensions*, vol. 149, no. 012039, 2009, p. 4.
[32] V. C. Barroso, H. Raich, P. Blömler, and M. Wilhelm, "Double dipolar Halbach array for rheological measurements on magnetic fluids at variable magnetic flux density B," in *Proc. 11th Conf. Electrorheological Fluids Magnetorheological Suspensions*, vol. 149, no. 012102, 2009, p. 4.
[33] A. Wiehe and J. Maas, "Magnetorheological actuators with currentless bias torque for automotive applications," *J. Intell. Mater. Syst. Struct.*, vol. 21, pp. 1575–1585, Oct. 2010.
[34] B. Yang, T. Chen, G. Meng, Z. Feng, J. Jiang, S. Zhang, and Q. Zhou, "Design of a safety escape device based on magnetorheological fluid and permanent magnet," *J. Intell. Mater. Syst. Struct.*, vol. 24, pp. 49–60, Jan. 2013.
[35] H.-U. Oh, "Characteristics of a magnetorheological fluid isolator obtained by permanent magnet arrangement," *Smart Mater. Struct.*, vol. 13, no. 3, pp. 29–35, 2004.
[36] G. Armenio, E. Bartalesi, F. Bucchi, A. Ferri, P. Forte, F. Frendo, R. Rizzo, and R. Squarcini, "Mechanical combustion engine driven fluid pump," EPO Patent 11 425 176.2-2423, 2011.
[37] E. Bartalesi, F. Bucchi, and R. Squarcini, "Vacuum actuation for axial movement of a magnet in a magnetorheological clutch," EPO Patent Pending.
[38] G. L. Johnston, W. C. Kruckemeyer, and R. E. Longhouse, "Passive magnetorheological clutch," U.S. Patent 5 848 678, Dec. 15, 1998.
[39] T. Saito and H. Ikeda, "Development of normally closed type of magnetorheological clutch and its application to safe torque control system of human-collaborative robot," *J. Intell. Mater. Syst. Struct.*, vol. 18, no. 12, pp. 1181–1185, Dec. 2007.
[40] G. Aydar, X. Wang, and F. Gordaninejad, "A novel two-way-controllable magnetorheological fluid damper," *Smart Mater. Struct.*, vol. 19, no. 6, pp. 1–7, 2010.
[41] F. Bucchi, P. Forte, F. Frendo, A. Musolino, and R. Rizzo, "A fail-safe magnetorheological clutch excited by permanent magnets for the disengagement of automotive auxiliaries," *J. Intell. Mater. Syst. Struct.*. Jan, 2014. doi: 10.1177/1045389X13517313.
[42] Lord Corporation. (2013). [Online]. Available: http://www.lord.com
[43] *EFFE v2.00, User Manual*, Bathwick Electrical Design Ltd., Bath, U.K., Jan. 2009.
[44] F. Bucchi, P. Forte, F. Frendo, and R. Squarcini, "A magnetorheological clutch for efficient automotive auxiliary device actuation," *Fract. Struct. Integrity*, vol. 23, pp. 62–74, 2013.
[45] LORD 5 Nm TFD Steer-By-Wire Device. [Online].Available:http://www.lord.com/products-and-solutions/magneto-rheological-(mr)/product.xml/1650/2

Rocco Rizzo received the Ph.D. degree in electrical engineering from the Department of Electrical Systems and Automation, University of Pisa, Pisa, Italy, in 2002.

He is currently an Assistant Professor of Electrical Engineering at the University of Pisa. He has published more than 80 papers in international journals and refereed conferences. His research interests include the development of analytical and numerical methods for the analysis of electromagnetic fields in linear and nonlinear media applied to the design of electromagnetic devices for special purposes.

Dr. Rizzo has been a Member of the Academy of Nonlinear Sciences, Russia, since 2004.

Antonino Musolino is an Associate Professor of Electrical Engineering at the University of Pisa, Pisa, Italy. His research interests include the development of analytical and numerical techniques for the analysis of electromagnetic fields in linear and nonlinear media. He is author of more than 100 papers on international journals and conferences.

Prof. Musolino has served as Vice General Chairman, Session Organizer, and Member of editorial boards for several international conferences, including Applied Computational Electromagnetics Society Symposium, Progress in Electromagnetics Research Symposium, and Conference on Electromagnetic Field Computation.

Francesco Bucchi received the Ph.D. degree in mechanical engineering from the University of Pisa, Pisa, Italy, in 2014.

He is currently a Research Fellow in the Department of Civil and Industrial Engineering, University of Pisa. His research interests include the mechanical properties of materials and multibody simulation of different types of vehicles.

Paola Forte received the degree in mechanical engineering (*cum laude*) in 1981 and the Ph.D. degree in tribology from the University of Pisa, Pisa, Italy, in 1989.

Before joining the academic staff of the University of Pisa as an Assistant Professor of Machine Design in 1992, she worked as a Design Engineer in the private industry of automotive components and as a Teacher of technical drawing. Since 2002, she has been an Associate Professor of Machine Design at the University of Pisa. Her research activity is documented by more than 145 scientific papers in national and international journals and conference proceedings, and four patents. Her research interests include dynamics of machines, vibroacoustics, and structural analysis, with particular attention to biomechanics.

Francesco Frendo received the Graduate degree (*cum laude*) in nuclear engineering and the Ph.D. degree in mechanics of materials in 1998 from the University of Pisa, Pisa, Italy.

He started his professional career as an Assistant Professor in Machine Design in 2000. Since December 2011, he has been an Associate Professor of Machine Design at the University of Pisa. He is a coauthor of more than 100 scientific papers published in international journals and conferences.

Dr. Frendo received a National Award from the Italian Association for Stress Analysis for a paper presented at a national conference in 2000. In 2008, he received two Special Recognition Awards from the Society of Automotive Engineers for two papers presented at the Small Engine Technology 2008 Conference.